Density-functional theory of the magnetic anisotropy of nanostructures: an assessment of different approximations

2009 J. Phys.: Condens. Matter 21 426001

(http://iopscience.iop.org/0953-8984/21/42/426001)

IOP PUBLISHING JOURNAL OF PHYSICS: CONDENSED MATTER

J. Phys.: Condens. Matter **21** (2009) 426001 (12pp) doi:10.1088/0953-8984/21/42/426001

Density-functional theory of the magnetic anisotropy of nanostructures: an assessment of different approximations

Piotr Błoński and Jürgen Hafner[1]

Fakultät für Physik and Center for Computational Materials Science, Universität Wien, Sensengasse 8/12, A-1090 Wien, Austria

E-mail: juergen.hafner@univie.ac.at

Received 16 July 2009, in final form 27 August 2009
Published 29 September 2009
Online at stacks.iop.org/JPhysCM/21/426001

Abstract

We discuss the multiple technical choices that have to be made in *ab initio* density-functional calculations of the magnetic anisotropy of supported nanostructures: (i) choice of the exchange–correlation functional, (ii) degree of optimization of the geometry of the adsorbate/substrate complex, (iii) magnetic anisotropy energy calculated self-consistently or via the 'force theorem', (iv) calculations based on slab models of the substrate or using a Green's function describing a semi-infinite substrate, (v) full potential approach or atomic-sphere approximation. Using isolated Fe and Co atoms on Pt(111) as an example we demonstrate that by using a judicious combination of relatively crude approximations (complete neglect of structural relaxation, local exchange–correlation functional, . . .) seemingly good agreement with experimental anisotropy energies can be achieved, while the calculated orbital moments remain small. At a higher level of theory (relaxed adsorbate/substrate complex, gradient-corrected functionals, . . .) providing a realistic geometry of the adsorbate/substrate complex and hence a correct description of the interaction between the magnetic adatom and its ligands, anisotropy energies are also in semi-quantitative agreement with experiment, while the orbital moments of the adatoms are much too small. We suggest that the anisotropy energies provided by both approaches should be considered as lower limits of the real anisotropies. Without relaxation the ligand effect coupling the orbital moments of the adatom to the heavy atoms of the substrate is underestimated, while in a relaxed adsorbate/substrate complex the lack of orbital dependence of the exchange potential combined with a strong hybridization of adatom and substrate states leads to a strong underestimation of the orbital moment. We have briefly explored the influence of post-density-functional corrections. Adding a modest on-site Coulomb repulsion to the d states of the adatom (in a DFT + U approach) leads to a modest increase of spin and orbital moments of the adatom accompanied by a slow decrease of the induced moments, leaving the anisotropy energy almost unchanged.

(Some figures in this article are in colour only in the electronic version)

1. Introduction

Recently there has been great interest in the magnetic anisotropy energy (MAE) of small magnetic nanostructures supported on nonmagnetic substrates, motivated by the desire to build magnetic or magneto-optical memory storage devices with a maximal storage density [1]. A high magnetic anisotropy is required to inhibit magnetization reversal—the critical value of the MAE is about 1.2 eV/bit. Therefore a reduction of the size of the nanostructures carrying one bit of information requires an increase of the MAE per atom. In addition the dipolar magnetic interactions between neighboring bits must be sufficiently weak, and this can be achieved if the easy axis of magnetization is perpendicular to the plane of the

[1] Author to whom any correspondence should be addressed.

substrate. The ultimate limit of a system showing magnetic anisotropy is an isolated atom on a nonmagnetic substrate. A high magnetic anisotropy energy requires large spin and orbital magnetic moments and a strong spin–orbit coupling. Large spin moments are found among the ferromagnetic 3d metals Fe and Co, but for these elements the orbital moment is small and the spin–orbit coupling is weak. Strong spin–orbit coupling is found in the heavy 5d metals, but these elements are nonmagnetic. Nanostructures of 3d metals supported on substrates of highly polarizable 5d metals are a viable route to tune both the spin moments and the anisotropy energy, and the simplest such nanostructure is of course an isolated magnetic atom on a substrate.

Using x-ray magnetic circular dichroism (XMCD) (see, e.g. Stöhr [2] and further references cited therein) it is now possible to measure the magnetic properties of adsorbed species down to surface coverages as low as 0.002 ML, extracting the spin and orbital moments as well as the magnetic anisotropy energy. However, because the focus of the x-ray beam is of the order of a few hundred μm^2, the experiment provides spatially averaged information. Consequently, information on the properties of single atoms or on well defined nanoclusters can only be achieved if surfaces with a homogeneous distribution of single atoms or monodisperse clusters can be prepared. A review of experimental investigations of the magnetism of individual atoms adsorbed on surfaces has recently been presented by Brune and Gambardella [3]. The results for isolated Co atoms on Pt(111) are characteristic for the magnetism of 3d atoms on highly polarizable substrates composed by 4d or 5d metals [3, 4]. The effective spin moment of $\mu_S^{\rm eff} = 1.8 \pm 0.1\ \mu_{\rm B}$ and the orbital moment of $\mu_L = 1.1 \pm 0.1\ \mu_{\rm B}$ measured at $T = 5.5$ K and in a magnetic field of $B = 7$ T sufficient to achieve saturation are both strongly enhanced not only compared to bulk Co (where $\mu_S = 1.52\ \mu_{\rm B}$ and $\mu_L = 0.15\ \mu_{\rm B}$), but also compared to 2D films [5–7], 1D atomic wires [8, 9], and supported nanoclusters [7, 10]. From the variation of the magnitude of the XMCD relative to the x-ray adsorption intensity measured for a magnetic field perpendicular ($\theta = 0°$) and nearly parallel ($\theta = 70°$) to the surface, a very large magnetic anisotropy of MAE $= 9.3 \pm 1.6$ meV was estimated. This extraordinarily large MAE has to be attributed to the reduced coordination of the Co atom and to the magnetic moments induced in the Pt substrate combined with the strong spin–orbit coupling of the Pt 5d states. The strong polarization of the substrate atoms is a consequence of the strong Stoner enhancement factor of Pt. For an isolated Co atom on the Pt(111) surface an effective moment of $\mu_S = 5.0 \pm 0.6\ \mu_{\rm B}$ has been estimated—this is comparable, but still lower than the effective 'giant moment' of 10 $\mu_{\rm B}$ reported for Co atoms in very dilute Co–Pt alloys [11]. This large difference in the effective moments suggests that the coordination of the magnetic impurity by the polarizable atoms is of decisive importance for the strong enhancement of the MAE of the Co atom by the coupling to the ligands.

Complementary investigations of isolated Co atoms have been performed using spin-polarized scanning tunneling microscopy (STM) and scanning tunneling spectroscopy (STS) [12]. The STM images show that the Co atoms occupy both fcc and hcp hollows of the Pt substrate. The differential conductance dI/dV derived from the STS experiment shows no sign of hysteresis down to the lowest temperatures. This has been attributed to magnetization reversal by quantum tunneling. The curves may be fitted as a function of the magnetic field and its angle relative to the magnetic moment of the atom. Assuming an out-of-plane easy axis and MAE $=$ 9.3 meV the fit yields effective magnetic moments of μ(hcp) $= 3.9 \pm 0.2\ \mu_{\rm B}$ and μ(fcc) $= 3.5 \pm 0.2\ \mu_{\rm B}$ for the two adsorption sites, respectively. The STM studies also suggest a weak coupling between the Co-moments mediated by the conduction electrons of the substrate.

Very recently it has been claimed [13] that the STS experiments providing information on the spin-flip energy $E_{\rm sf}$ (i.e. on the energy required to change the magnetic adatom from its ground state with spin $\pm S$ to a state with $\pm(S-1)$) can also be used to obtain the MAE. If the spin is known, the MAE is approximated as $E_{\rm sf} \times S^2/(2S-1)$. Although in their analysis Balashov *et al* [13] have ignored the fact that the spin to be flipped is not the spin of the adatom alone, but the effective spin of the adatom/substrate complex, they find for Co/Pt(111) an MAE of 10.25 meV/atom in good agreement with Gambardella *et al* [4]. For an isolated Fe atom on Pt(111) again a perpendicular anisotropy and a large MAE of 6.53 meV/atom has been reported.

Experiments using XMCD and x-ray adsorption spectroscopy (XAS) on isolated Fe atoms on Pt(111) revealed a much lower ratio for orbital to effective spin moment of $L/S_{\rm eff} \sim 0.18 \pm 0.05$ (to be compared to $L/S_{\rm eff} \sim 0.61 \pm 0.05$ for Co/Pt(111)), an out-of-plane orientation of the easy axis and a very low MAE [14]. Similar values have been reported for very small Fe_n clusters ($n = 2 \rightarrow 9$) adsorbed on ultrathin Ni films supported on a Cu(100) substrate [15]. For clusters of this size the ratio $L/S_{\rm eff}$ varies between 0.08 (for $n = 3$) and 0.27 (for $n = 6$).

These experiments have also motivated theoretical studies of the magnetism of supported isolated atoms based on spin-density-functional techniques [4, 16–24]. The calculation of the magnetic anisotropy is a problem of fundamental importance. Magnetic anisotropy, magneto-optical spectra, magnetic dichroism, and other important properties are caused by spin–orbit coupling, hence a relativistic calculation is required. A further complication arises from the fact that whereas spin magnetic moments are described quite accurately by density-functional theory (DFT) based on semilocal, gradient-corrected exchange–correlation functionals, the orbital moments are generally underestimated. The reason is that the variables determining the effective one-electron potential within DFT (the charge and spin densities) are determined as averages over occupied orbitals. It has been suggested that the prediction of the orbital moments should be improved by adding post-DFT calculations such as the empirical orbital polarization term proposed by Brooks *et al* [25, 26] or using the DFT $+ U$ method [27, 28] adding an on-site Coulomb repulsion U to the potential acting on the d-electrons of the magnetic atom [4, 23]. However, calculations using the full orbital polarization term tend to

produce too large orbital moments [4]. For adatoms supported on strongly polarizable substrates it is also evident that a very accurate determination of the geometry of the adatom/substrate complex is required.

Indeed a calculation of the magnetic anisotropy energy requires a number of technical choices, involving the following.

(i) The choice of an exchange–correlation functional, i.e. local spin-density approximation (LSDA) or generalized-gradient approximation (GGA). GGA calculations not only produce slightly larger (and in general more accurate) lattice constants and magnetic moments than the LSDA, but for bulk Fe the GGA is also mandatory for a correct prediction of the ground state [29].
(ii) Post-DFT corrections (orbital polarization, on-site Coulomb repulsion, ...) which are added to the exchange–correlation functional.
(iii) Self-consistent electronic structure calculations, including spin–orbit coupling, using projector-augmented wave (PAW) [30, 31] or full potential linearized augmented wave (FLAPW) codes [32], or using multiple-scattering (screened Kohn–Korringa–Rostocker—SKKR) [34] calculations. This also implies different treatments of the effective potentials. PAW and FLAPW provide a full potential approach, while SKKR calculations rely on the atomic-sphere approximation. The spherical averaging over the atomic sphere of the adatom certainly reduces the effect of the broken symmetry of the adatom.
(iv) Modeling of the substrate: periodic slab models or semi-infinite substrate (possible only within Green's function SKKR). However, it has to be emphasized that in Green's function calculations the Dyson equation for the perturbed system is solved only for an embedded cluster surrounding the magnetic adatom which is usually smaller than the unit-cell in a slab model.
(v) Geometry of the adsorbate/substrate complex: all atoms on ideal sites continuing the crystalline lattice of the substrate (complete neglect of relaxation), relaxation of the position of the adatom only, or full relaxation of adatom plus surface.
(vi) MAE calculated as the difference in the total energies from self-consistent calculations for different orientations of the magnetic moment or, using the 'magnetic force theorem' [35] as the difference in the band energies at a fixed potential and charge density.

Using a judicious combination of different approximations (ideal bulk-like geometry—no relaxation of either adatom or surface, local spin-density approximation—no gradient corrections, atomic-sphere approximation for the effective potential within SKKR calculations, MAE calculated via the 'magnetic force theorem') quite reasonable values for the MAE can be achieved, while the calculated orbital moments are somewhat too low [4, 17, 20, 22]. However, whether these approximations are also adequate has never been questioned. Attempts have been made to cure the underestimation of the orbital moments by using an orbital polarization term—this results in moments which are now far too large [4, 23]. DFT + U calculations with a modest on-site repulsion of $U = 2 \rightarrow 3$ eV lead to a better agreement with experiment, but since the choice of U is open, this is a semiempirical approach [33]. The relaxation of the adatom–substrate complex has been calculated by Spišák and Hafner [24]. It has been shown that this leads to the formation of a large polarization cloud and a very high effective spin moment per atom, but also to a strong quenching of the orbital moment of the adatom due to an increased hybridization with the substrate.

The intention of the present work is to provide a critical analysis of the impact of all these technical choices on the calculation of the magnetic anisotropy energy. Single Fe and Co adatoms on a Pt(111) surface are used as model systems, because both experimental [4, 13] and theoretical [4, 19–23] studies are available in the literature.

2. Computational details

We have used the Vienna *ab initio* simulation package VASP [31, 37] to perform *ab initio* electronic structure calculations and structural optimizations. VASP performs an iterative solution of the Kohn–Sham equations of DFT within a plane-wave basis and using periodic boundary conditions. Either local and semilocal functionals in the GGA [38], both combined with the spin-interpolation proposed by Vosko *et al* [39] can be used to describe electronic exchange and correlation and spin polarization. The use of a semilocal functional is known to be essential for the correct prediction of the ground state of the ferromagnetic 3d elements in the bulk [29]. The PAW method [30, 31] is used to describe the electron–ion interactions. The PAW approach produces the exact all-electron potentials and charge densities without elaborate nonlinear core-corrections—this is particularly important for magnetic elements.

The PAW potentials have been derived from fully relativistic calculations of the atomic or ionic reference calculations. Spin–orbit coupling has been implemented in VASP by Kresse and Lebacq [40]. Following Kleinman and Bylander [41] and MacDonald *et al* [42] the relativistic Hamiltonian given in a basis of total angular momentum eigenstates $|j, m_j\rangle$ with $j = l \pm \frac{1}{2}$ (containing all relativistic corrections up to order α^2, where α is the fine-structure constant) is recast in the form of 2×2 matrices in spin-space by re-expressing the eigenstates of the total angular momentum in terms of a tensor product of regular angular momentum eigenstates $|l, m\rangle$ and the eigenstates of the z-component of the Pauli spin matrices. The relativistic effective potential consists of a term diagonal in spin-space which contains the mass-velocity and Darwin corrections, and the spin–orbit operator. The nondiagonal elements in spin-space arise from the spin–orbit coupling, but also from the exchange–correlation potential when the system under consideration displays a noncollinear magnetization density. Calculations including spin–orbit coupling have therefore to be performed in the noncollinear mode implemented in VASP by Hobbs *et al* [43] and Marsman and Hafner [44].

In our calculations the adatom–substrate complex has been described by a slab model. A five-layer slab with a 5×5

Table 1. The calculated adsorption energy E_{ad}, work function change $\Delta\Phi$ (with respect to the work function of the clean surface, $\Phi^{Pt} = 5.72$ eV), height z^x of adsorbed adatom above the Pt(111) surface, x-Pt bond length d^x, relaxations Δ_{ij} of the interlayer distance, and the buckling of the Pt layers, b_i^{Pt}. X denotes either the Fe or Co adatom.

Adsorption site	E_{ad} (eV)	$\Delta\Phi$ (eV)	z^{x-Pt} (Å)	d^x (Å)	Δ_{12} (%)	Δ_{23} (%)	b_1^{Pt} (Å)	b_2^{Pt} (Å)
			Fe/Pt					
Fcc hollow	5.566	−0.40	1.71	2.39	+0.9	−1.2	0.12	0.08
Hcp hollow	5.561	−0.41	1.69	2.40	+0.9	−1.1	0.09	0.03
			Co/Pt					
Fcc hollow	5.736	−0.35	1.69	2.40	+1.1	−0.9	0.11	0.05
Hcp hollow	5.763	−0.31	1.62	2.46	+0.8	−1.1	0.07	0.13

surface cell has been used for describing the substrate, the adatom has been placed into the center of the surface cell. This means that the nominal surface coverage is 0.04 ML, coming close to the coverage of the samples on which the XMCD experiments have been performed. Neighboring slabs are separated by a vacuum region of 16 Å—this ensures that the separation between the periodically repeated images of the slab is large enough to suppress any interactions. The basis set contained plane waves with a maximum kinetic energy of 300 eV. Test calculations with higher cut-off energies have shown that this is a reasonable compromise between accuracy and computational effort. The calculations have been performed in two steps. First a collinear scalar-relativistic calculation has been performed to determine the correct geometry of the adatom/surface complex and the correct magnetic ground state. The ground state resulting from the scalar-relativistic calculations was used to initialize the noncollinear calculations including spin–orbit coupling which allow, in principle, a further structural optimization. Two independent self-consistent calculations (including a full structural re-optimization of the adatom/substrate complex) with the magnetic axis oriented perpendicular and parallel to the surface have been performed and the magnetic anisotropy energy has been calculated as the difference in the well-converged total energies. Alternatively, the magnetic force theorem has been used to determine the MAE. Brillouin-zone integrations have been performed on $3 \times 3 \times 1$ grids, using a modest smearing to improve convergence. Test calculations with finer grids have shown that for this large supercell this leads to converged results. Final total energies are extrapolated to zero smearing. Geometric, electronic, and magnetic degrees of freedom are relaxed simultaneously until the forces acting on all atoms converge below 0.01 eV Å^{-1} and the changes in total energy between successive iteration steps are smaller than 10^{-7} eV—such a stringent relaxation criterion was found to be absolutely essential.

3. Results

3.1. Structure of clean Pt(111) surfaces

For bulk face-centered cubic Pt we calculate using the GGA a lattice constant of $a = 3.993$ Å and a bulk modulus of $B = 236$ GPa, in the LDA the corresponding values are $a = 3.910$ Å and $B = 286$ GPa, to be compared with the experimental values of $a = 3.924$ Å and $B = 230$ GPa [45]. As for all heavy elements, the lattice constant calculated using the GGA is too large by about 1.5% while the LDA value is too low. The bulk modulus, however, is definitely more accurate if calculated using the GGA. For the characterization of the (111) surface, the three top layers of the slab have been allowed to relax, while the lower two layers are kept frozen in their bulk-like positions. The relaxation leads to an expansion of the distance between the two top layers by $\Delta_{12} = 0.7\%$, while the distance between the subsurface layers is contracted by $\Delta_{23} = -1.4\%$. The predicted surface expansion is in good agreement with the LEED data of $\Delta_{12} \sim 1\%$ [47]. For the work function we find a value of $\Phi = 5.72$ eV, again in very good agreement with experiment ($\Phi = 5.6 \rightarrow 6.4$ eV) [46]. The calculations have been performed in a spin-polarized mode, initializing the magnetic moments of the surface atoms to non-zero values. However, the calculations always converged to a completely nonmagnetic solution, demonstrating that no spurious surface magnetism is induced by the reduced coordination of the surface atoms.

3.2. Fe and Co adatoms on Pt(111) surfaces

For the isolated adatom on the Pt(111) surface we have considered a location either in an fcc or in an hcp hole. The results for the adsorption geometry, the relative energy, and for the work function change from scalar-relativistic spin-polarized calculations are compiled in table 1.

For an isolated Fe atom, adsorption in an fcc hollow leads to an adsorption energy which is larger by 5.5 meV than for adsorption in an hcp hollow. The height of the Fe atom above the top Pt layer is 1.71 Å—this is reduced by 0.595 Å or 26% compared to the ideal interlayer distance in bulk Pt and corresponds to a reduction of the shortest Fe–Pt distance from 2.82 to 2.39 Å. The reduced height of the Fe adatom above the Pt surface is primarily a consequence of the large size-misfit between Fe and Pt and the desire to maintain an effective volume close to the equilibrium value in the bulk. Given the in-plane lattice constant of Pt(111) and the height of the Fe atom, we calculate an atomic volume of 11.81 Å^3 which is only slightly increased compared to bulk bcc Fe. Even this very low Fe-coverage leads to a slightly increased outward-relaxation of the distance between the top Pt layer. The adatom also induces a slight buckling of the top layers, the Pt atoms binding to the Fe atoms move outwards towards the adatom by about 0.12 Å.

Table 2. Spin μ_S, orbital μ_L, and total $\mu_{\rm tot}$ magnetic moments (all in $\mu_{\rm B}$) of Fe and Co adatoms adsorbed on a Pt(111) substrate and induced moments on the Pt-substrate atoms integrated over all atoms in the supercell. Results from scalar-relativistic calculations and including spin–orbit coupling for perpendicular and in-plane orientations of the magnetic moment are presented. The MAE is given in meV, a positive value indicates a perpendicular easy axis. The calculations are performed using the GGA and allow for a full relaxation of the adatom/substrate complex.

	Scalar-relativistic	Including SOC						
		Perpendicular			In-plane			
	μ_S	μ_S	μ_L	$\mu_{\rm tot}$	μ_S	μ_L	$\mu_{\rm tot}$	MAE
Fe (fcc hollow)	3.306	3.282	0.104	3.386	3.283	0.108	3.391	
Pt	2.377	2.153	0.402	2.555	2.172	0.518	2.690	
Effective moment	5.683	5.435	0.506	5.941	5.455	0.626	6.081	2.99
Experiment, [14] Fe								$\geqslant 0$
Experiment, [13] Fe								6.5 ± 0.1
Co (hcp hollow)	2.190	2.155	0.126	2.281	2.155	0.088	2.243	
Pt	4.826	3.319	0.684	4.003	3.325	0.829	4.154	
Effective moment	7.016	5.474	0.810	6.284	5.480	0.917	6.397	1.19
Experiment, [4] Co		2.1	1.1	3.2				9.3 ± 1.6
Experiment, [13] Co								10.3 ± 0.2

The work function is reduced by 0.4 eV—a surprisingly strong effect at such a low concentration of adatoms. This may be understood in terms of the strong adatom–substrate interaction, the large magnetic moment of the adatom and the long-range magnetic polarization induced in the substrate (see below for details).

For a Co atom, adsorption in an hcp hollow is strongly preferred over the fcc hollow, by 27.9 meV. A Co atom in an hcp hollow moves even closer to the Pt substrate (the height of the adatom is reduced by 29.7% compared to the idealized lattice position) the adsorption-induced outward-relaxation is very modest. The stronger relaxation results from an attractive interaction with a Pt atom in the subsurface layer, which is also reflected in a buckling of this layer which is more pronounced in the subsurface than in the surface layer. Shick *et al* [23] have used an LSDA+U approach (with $U = 2$ eV) to determine the equilibrium height of a Co adatom at a fixed bulk-like geometry of the substrate and report a smaller relaxation by about 20%.

3.3. Magnetic moments and magnetic anisotropy

In the following we report the results of our calculations of the magnetic moments and magnetic anisotropies of Fe and Co atoms on Pt(111) substrates, calculated at different levels of theory. We begin with the results compiled in table 2, obtained for a fully relaxed adatom/substrate complex, using the spin-polarized GGA and the MAE calculated from the total-energy differences calculated self-consistently for in-plane and perpendicular orientation of the magnetic moments. For both orientations of the magnetic moments we have also allowed a complete relaxation of the geometry. However, changes in the interatomic distances with the re-orientation of the magnetization direction are very small, of the order of 0.001 Å. Within a density-functional approach, this represents the highest level of theory.

3.3.1. Relaxed geometry of adatom/substrate complex. For an isolated Co atom in an hcp hollow on Pt(111) we find a strongly enhanced spin moment of 2.15 $\mu_{\rm B}$, slightly higher than the experimental estimate of Gambardella *et al* [4], while the calculated orbital moment is much too low. The magnetic atom induces a strong polarization of the substrate. Figure 1 shows for Co/Pt(111) the induced spin and orbital moments in the three top layers of the substrate, calculated for perpendicular and in-plane orientation of the magnetization. The distribution of the induced moments is similar for Fe/Pt(111). The figure demonstrates that although the induced magnetization decays rapidly in the deeper layers, the decrease of the induced moments in the top layer with increasing distance from the adatom is slower, such that even at this low coverage the induced magnetization clouds overlap slightly. On the Pt atoms that are nearest neighbors to the Co (Fe) adatom the ratio μ_L/μ_S is 0.25(0.20) for perpendicular and 0.31(0.24) for in-plane magnetization, respectively. Hence the ratio of orbital to spin moment is much higher than for the adatom, as expected because of the stronger spin–orbit coupling.

An interesting question is also the change in the magnetization densities of adatom and substrate induced by their interaction and the small changes in the magnetization densities induced by the re-orientation of the direction of the magnetic moment. This is illustrated in figure 2 showing for Fe/Pt(111) the difference in the magnetization densities of the adatom/substrate complex and of the isolated atom plus the clean substrate. Both calculations refer exactly to the same geometry, i.e. the clean surface has been deformed such as under the influence of the adatom and the magnetization density of the free atom is centered around the relaxed adatom position. Contours of regions with increased/decreased magnetization densities are shown. The gross features of

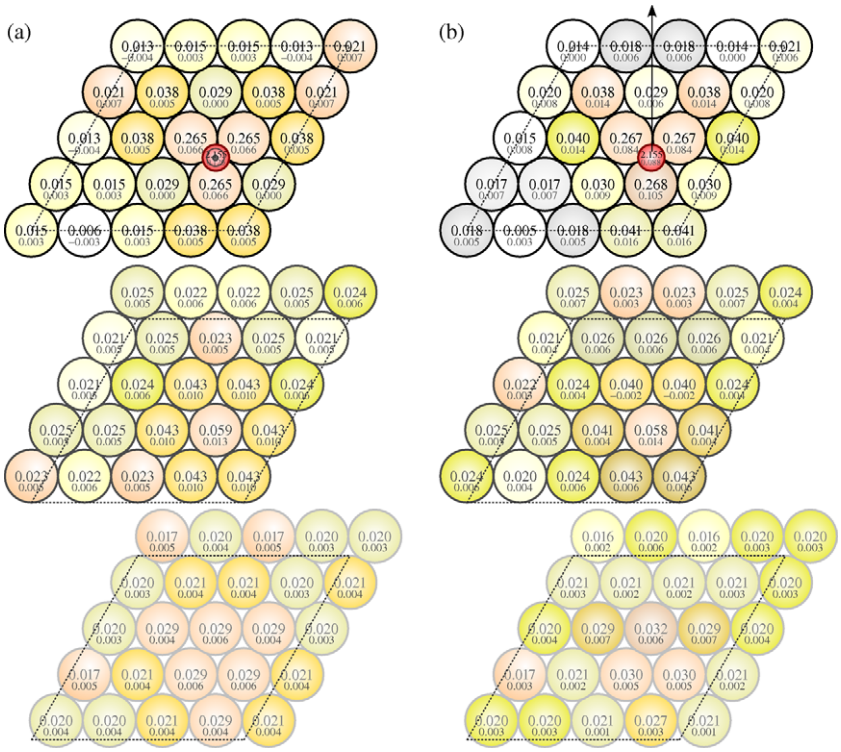

Figure 1. Spin and orbital moments induced by a Co adatom in a hcp hollow of a Pt(111) surface in the top three layers of the substrate. For each atom the top (larger) number gives the induced spin moment, the lower (smaller) number the induced orbital moment. Both are given in μ_B. Part (a) refers to perpendicular, part (b) to in-plane magnetization (as indicated by the large arrows).

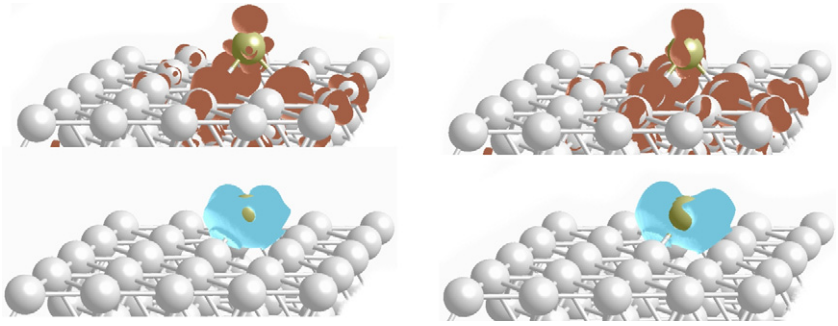

Figure 2. Constant-density surfaces showing the difference-magnetization densities for an Fe atom adsorbed in an fcc hollow on a Pt(111) surface. The upper panels (brown surfaces) show regions of increased magnetization densities visualizing the induced magnetic polarization of the substrate, but also regions of increased magnetization around the adatom. The lower panels (blue surfaces) show the regions of reduced magnetization around the adatom. The contour values are ± 0.0075 electrons Å^{-3}. The left panels refer to perpendicular, the right ones to in-plane magnetization (compare with text).

the plots demonstrate the reduced magnetic moment of the adatom relative to the large moment of the free atom and the induced polarization of the substrate. Surprisingly, there are also small regions of increased magnetization density around the adatom, extending mostly in a perpendicular direction. Most interesting in connection with the magnetic anisotropy are the small changes in these magnetization densities upon re-orientation of the magnetic axis. These changes reflect the broken symmetry for in-plane orientation.

The induced magnetization (integrated over all substrate atoms) is lower than in a scalar-relativistic calculation, because the strong spin–orbit coupling mixes different spin states. The integrated induced orbital moment is much larger than the orbital moment of the magnetic adatom and it is also much more anisotropic—in both cases the induced orbital moment is much larger for in-plane magnetization while the spin anisotropy is only modest. Interestingly, the effective spin moment per Co atom of about 5.5 μ_B is in very good agreement with the estimated effective moment of $5.0 \pm 0.6\ \mu_B$. From the difference in the total energies we deduce a magnetic anisotropy energy of 1.2 meV favoring a perpendicular easy axis of magnetization. The sign of the MAE agrees with the anisotropy of the orbital moments of the Co atoms and of the induced orbital moments and with experiment, although we find a much lower value than deduced from the XMCD experiments or estimated from the STS spectra. Our MAE of

Table 3. Spin μ_S, orbital μ_L, and total μ_{tot} magnetic moments (all in μ_B) of Fe and Co adatoms adsorbed in a fcc hollow on a Pt(111) substrate and induced moments on the Pt-substrate atoms integrated over all atoms in the supercell. Results including spin–orbit coupling for perpendicular and in-plane orientations of the magnetic moment are presented. The MAE is given in meV, a positive value indicates a perpendicular easy axis. The calculations are based on an idealized bulk-like geometry (using the experimental lattice constant) and use either the GGA or the LSDA functional.

	Including SOC						
	Perpendicular			In-plane			
	μ_S	μ_L	μ_{tot}	μ_S	μ_L	μ_{tot}	MAE
Fe—LSDA, present work							
Fe	3.366	0.343	3.709	3.366	0.234	3.600	
Pt	1.363	0.227	1.590	1.457	0.325	1.782	
Effective moment	4.729	0.570	5.299	4.823	0.559	5.382	2.35
Fe—LSDA, [22]							
Fe	3.395	0.628	4.023	3.514	0.266	3.780	5.31
Fe—LSDA, [19]							
Fe	3.49	0.77	4.26				8.79
Experiment, [14]							
Fe							$\geqslant 0$
Experiment, [13]							
Fe							6.5 ± 0.1
Co—LSDA, present work							
Co	2.152	0.631	2.783	2.151	0.350	2.501	
Pt	1.135	0.194	1.329	1.258	0.279	1.537	
Effective moment	3.287	0.825	4.112	3.409	0.629	4.038	8.14
Co—GGA, present work							
Co	2.195	0.431	2.626	2.195	0.246	2.441	
Pt	1.605	0.282	1.887	1.769	0.395	2.164	
Effective moment	3.800	0.713	4.513	3.964	0.641	4.605	2.42
Co—LSDA, [22]							
Co	2.153	0.726	2.879	1.973	0.483	2.456	5.02
Co—LSDA, [19, 20]							
Co	2.27	0.60	2.87				4.76
Pt	0.40	0.07	0.47				
Co—LSDA, [23]							
Co	2.18	0.57	2.75				2.00
Co—LSDA, [4]							
Co	2.14	0.60	2.74				18.45
Experiment, [4]							
Co	2.1	1.1	3.2				9.3 ± 1.6
Experiment, [13]							
Co							10.3 ± 0.2

1.2 meV is also lower than the theoretical predictions derived for an unrelaxed surface [19, 22], a detailed discussion of the difference will be given below.

For an Fe adatom the enhancement of the spin moment compared to its value in the bulk is even more pronounced, but we find an orbital moment which is only slightly enhanced compared to the bulk. For the adatom the ratio μ_S/μ_L is only about 0.03, much smaller than the experimental estimate of $\mu_S/\mu_L \sim 0.18 \pm 0.05$ given by Lehnert [14]. For the substrate atoms, this ratio is much higher—$\mu_L/\mu_S \sim 0.20(0.29)$ for perpendicular (in-plane) magnetization. Although the anisotropy of both spin and orbital moments is very small, we calculate an MAE of 3 meV—the out-of-plane easy axis agrees with the easy axis direction found by Lehnert (no quantitative MAE could be deduced) and with the value of 6.5 meV estimated by Balashov *et al* [13] from the STS. Much larger values of the MAE have been predicted by Bornemann *et al* [19] and Etz *et al* [22], based on an ideal geometry and an LSDA functional. Tsujikawa *et al* [21] studied the MAE of a quarter of a monolayer of Fe on Pt(111) within the LSDA and allowing a restricted relaxation. An in-plane easy axis favored by about 1 meV was reported, although spin and orbital moments are not too different from our results.

3.3.2. Idealized geometry of the adatom/substrate complex. To allow a comparison of our calculations with the existing literature data, we have also performed calculations using a fixed idealized geometry based on the experimental lattice constant and either the LSDA or GGA exchange–correlation functional. In these calculations both Fe and Co have been placed into fcc hollows because this is the adsorption site assumed in the previous calculations. The results are compiled in table 3.

The LSDA calculations for Co/Pt(111) and a perpendicular orientation of the magnetic moment lead to good agreement with the published data [4, 19, 22, 23]: the spin moment of the Co atom is $\mu_S \sim 2.15 \pm 0.03\ \mu_B$, the orbital moment $\mu_L \sim 0.60 \pm 0.03\ \mu_B$ (but note that Bornemann *et al* [19] find a higher spin, and Etz *et al* [22] a higher orbital moment—these divergences are not easily understood because [4, 19] and [22] all use an SKKR Green's function code). We note that at a fixed geometry and with the same functional as in the present PAW calculations, the FLAPW calculations of Shick *et al* [23] (both using a slab model) and the SKKR calculations [4] based on a semi-infinite substrate (but solving the Dyson equation only in a finite surrounding of the adatom) lead to good agreement. Hence the two types of models are both adequate, and the difference between full potential and atomic-sphere approximations is not so important. Much larger differences are found for Fe/Pt(111)—we shall come back to this discrepancy below.

Compared to the calculations for a fully optimized adatom/substrate complex we find a strong enhancement of the orbital moment of the adatom and a pronounced decrease of both spin and orbital moments induced in the substrate. The effective spin moments per Fe or Co adatom are reduced from about 5.5 μ_B to ~3.3–3.4 μ_B, while the effective orbital moments are almost unchanged. In the previous publications information on the magnetic moments induced on the substrate atoms is very scarce. Etz *et al* [22] report induced spin moments of $\mu_S \sim 0.1\ \mu_B$ for the nearest-neighbor Pt atoms, decreasing to about 0.01 μ_B for next-nearest neighbors, Bornemann *et al* [19] report slightly lower induced spin moments of 0.08 μ_B on nearest-neighbor sites. These values are in reasonable agreement with our findings, but hardly any information on the induced orbital moments can be found in earlier work. Only Bornemann *et al* [19] report a total induced spin moment of 0.4 μ_B and a total induced orbital moment of 0.07 μ_B for Co/Pt(111) (both per Co atom). As these values are considerably lower than our integrated values while the moments induced on nearest-neighbor sites are comparable, we can only conclude that the spatial extension of the induced polarization cloud is much smaller than derived here. This is an immediate consequence of the fact that the Dyson equation has been solved only for a small cluster surrounding the adatom. On all other substrate atoms any induced polarization has hence been suppressed

Very little information has also been given on the anisotropies of spin and orbital moments—only in the paper by Etz *et al* [22] are values of the magnetic moments given for both orientations of the magnetization. The reason for the lack of information on the direction-dependence of the magnetic moments is that the calculations of the MAE use either the magnetic force theorem [4, 22, 23] or the torque–force approach [19, 20]. In both cases, a self-consistent calculation is performed only for one direction of the magnetization and the MAE is determined as the difference in the sum of the one-electron energies, calculated at a fixed effective one-electron potential. For Fe/Pt(111) our calculations predict an isotropic spin moment and a modest anisotropy of the orbital moment of the Fe atom, $\Delta\mu_L = \mu_l(\perp) - \mu_L(\parallel) = 0.11\ \mu_B$, and an orbital anisotropy of opposite sign, $\Delta\mu_L = -0.10\ \mu_B$ induced on the Pt atoms. For the Fe atom, Etz *et al* report a substantial negative anisotropy of the spin moments, $\Delta\mu_S = -0.12\ \mu_B$, and a very large orbital anisotropy of $\Delta\mu_L = 0.36\ \mu_B$. It is intriguing that for this system, the agreement between both sets of calculations is much better for an in-plane orientation of the magnetic moment. For Co/Pt(111) both calculations lead to similar values of the orbital anisotropy ($\Delta\mu_L \sim 0.2\ \mu_B$, but Etz *et al* also report a substantial negative spin anisotropy). The additional spin anisotropy is reflected in a MAE which is lower than found in our calculations. The MAE reported by Etz *et al* [22] agrees well with Bornemann *et al* [19], while Gambardella *et al* [4] report a much larger value (even larger than experiment). Since all three calculations [4, 19, 22] are based on a SKKR Green's function approach, the same geometry and the same functional, the origin of this difference is not clear. For Fe/Pt(111) the calculated MAEs span the range between 2 meV and nearly 9 meV. The difference between our low value and the larger values reported in the SKKR calculations parallels larger orbital moments and both orbital and spin anisotropies.

3.3.3. LSDA versus GGA. To assess the influence of the choice of the exchange–correlation functional, we have also performed calculations with an idealized geometry and a GGA functional. The results for Co/Pt(111) are listed in table 3. For the adatom, the semilocal GGA functional leads to a slightly increased spin and a significantly reduced and slightly less anisotropic orbital moment. In contrast the induced spin and orbital moments are significantly enhanced with the GGA, resulting also in an enhanced effective spin and orbital moment. As with the LSDA, we note opposite signs of spin and orbital anisotropies of the adatom and of the substrate. Altogether we note that the GGA disfavors the formation of a large orbital moment on the adatom, but also leads to stronger hybridization effects. Both effects together—decreased orbital anisotropy of the adatom and increased negative orbital anisotropy of the substrate—lead to a decrease of the magnetic anisotropy energy from 8.1 to 2.4 meV, while the sign remains unchanged.

3.3.4. Self-consistent total-energy differences versus force theorem. Calculations of the MAE require a very high level of convergence of the total energies—which is rather time-consuming. Therefore many calculations are based on the 'force theorem' [35, 36] stating that to first order, the difference in the total energy calculated for magnetization along the easy and hard axes may be approximated by the difference in the sum of the one-electron energies calculated at a fixed potential. If the force theorem has been used [4, 17, 22] a self-consistent calculation has been performed for perpendicular magnetization, while for in-plane magnetization only a non-self-consistent calculation with a fixed potential has been performed. In table 4 we compare the spin and orbital moments for in-plane orientation resulting from a self-consistent calculation and from a non-self-consistent calculation using the potential and charge-distribution resulting from the self-consistent calculation for

Table 4. Spin μ_S, orbital μ_L, and total $\mu_{\rm tot}$ magnetic moments (all in $\mu_{\rm B}$) of Fe and Co adatoms adsorbed on a Pt(111) substrate and induced moments on the Pt-substrate atoms integrated over all atoms in the supercell. Results for in-plane orientation of the magnetization resulting from self-consistent calculations and from non-self-consistent calculations based on the potentials and charge-distributions calculated for perpendicular magnetization are compared. The MAE is given in meV, a positive value indicates a perpendicular easy axis.

	Self-cons. total energy				Force theorem			
	μ_S	μ_L	$\mu_{\rm tot}$	MAE	μ_S	μ_L	$\mu_{\rm tot}$	MAE
Fe—GGA, relaxed, $a_{\rm theor.}$								
Fe	3.283	0.108	3.391		3.286	0.108	3.394	
Pt	2.172	0.518	2.690		2.163	0.514	2.677	
Effective moment	5.455	0.626	6.081	2.99	5.449	0.622	6.071	2.84
Fe—LSDA, ideal geometry								
Fe	3.366	0.234	3.600		3.378	0.236	3.614	
Pt	1.457	0.325	1.782		1.330	0.295	1.652	
Effective moment	4.823	0.559	5.382	2.35	4.708	0.531	5.239	2.31
Co—GGA, relaxed, $a_{\rm theor.}$								
Co	2.155	0.088	2.243		2.137	0.088	2.255	
Pt	3.325	0.829	4.154		3.279	0.812	4.091	
Effective moment	5.480	0.917	6.397	1.19	5.416	0.900	6.316	1.20
Co—LSDA, ideal geom.								
Co	2.151	0.350	2.501		2.137	0.354	2.491	
Pt	1.258	0.279	1.537		1.095	0.240	1.335	
Effective moment	3.409	0.629	4.038	8.14	3.232	0.594	3.826	12.71

perpendicular magnetization. Indeed we find that the non-self-consistent calculation reproduces the magnetic moments with very good accuracy. For Fe/Pt(111) we also find very good agreement between the MAEs calculated from the difference in the self-consistent total energies and determined by the difference in the sum of the one-electron energies (according to the force theorem), for both the GGA at a relaxed geometry, and the LSDA and the idealized bulk-like geometry. This is remarkable, because at the idealized geometry the differences between the self-consistently calculated induced moments and the non-self-consistent calculations are not entirely negligible. For Co/Pt(111) the force theorem yields good results in GGA calculations using a fully relaxed geometry, while in LSDA calculations for an idealized geometry the force theorem leads to value of the MAE which is increased by about 4 meV compared to the self-consistent result. The largest differences are always found for the induced spin moments, they are larger in LSDA calculations and larger for Co than for Fe adatoms. The reason is that at a fixed idealized geometry (and hence a partially suppressed hybridization) even small changes in the charge- and spin densities can lead to significant changes in the magnetic moments. This shows that the compensation between the changes in the one-electron energies and double-counting corrections (Hartree- and exchange–correlation energies) predicted by the force theorem is indeed realized in most cases to a very good extent, but the case of Co/Pt(111) demonstrates that for the very small MAEs the use of the force theorem can still lead to a non-negligible quantitative error.

3.3.5. DFT + U results. To examine the influence of post-DFT corrections on the orbital moment and on the MAE, we have performed calculations using a GGA + U approach and a modest value of $U = 2 \rightarrow 3$ eV for the on-site Coulomb repulsion on the Fe 3d states. For the implementation of the GGA + U approach in VASP we refer to the work of Rohrbach *et al* [48]. $U = 2$ eV is the value also used by Shick *et al* [23] in their calculations for Co/Pt(111) and slightly smaller than the value of $U = 3$ eV recommended by Ebert *et al* to achieve agreement for the orbital moments of 3d impurities in alloys. The calculations have been performed for a fully relaxed system. Our results are compiled in table 5. With increasing U we find increasing spin and orbital moments on the adatom, accompanied by a slow decrease of the induced moments. Both effects arise immediately from the increased exchange splitting of the Fe 3d states. The effect on the calculated MAR is also very modest.

The increase of the orbital moment of the adatom is much smaller than found by Ebert *et al* for 3d impurities in a polarizable matrix. The difference is again in the different treatment of relaxation effects. In the Green's function calculations of Ebert *et al*, local relaxations are neglected—hence the impurity couples only weakly to the host and the Coulomb repulsion induces a strong exchange splitting. In our relaxed system, the effect of the added Coulomb repulsion is much smaller because of the strong coupling to the ligand states.

Our results may be compared with the work of Shick *et al* [23] on Co/Pt(111), based on an LSDA + U approach on an unrelaxed or partially relaxed system. The Co orbital moments are more sensitive to the addition of a Coulomb repulsion, again the relaxation reduces its effect. Also the effect on the MAE is found to be small—with a $U = 2$ eV the MAE increases only from 2 to 3 meV. The use of the DFT+U method requires further investigations, including realistic estimates of the strength of the Coulomb repulsion.

Table 5. Spin μ_S, orbital μ_L, and total $\mu_{\rm tot}$ magnetic moments (all in $\mu_{\rm B}$) of Fe and Co adatoms adsorbed on a Pt(111) substrate and induced moments on the Pt substrate atoms integrated over all atoms in the supercell. Results from calculations including spin–orbit coupling for perpendicular and in-plane orientations of the magnetic moment are presented. The MAE is given in meV, a positive value indicates a perpendicular easy axis. The calculations are performed using the GGA + U and allow for a full relaxation of the adatom/substrate complex.

	Including SOC						
	Perpendicular			In-plane			
	μ_S	μ_L	$\mu_{\rm tot}$	μ_S	μ_L	$\mu_{\rm tot}$	MAE
	$U = 2$						
Fe	3.399	0.126	3.525	3.400	0.135	3.535	
Pt	2.103	0.392	2.495	2.192	0.524	2.716	
Effective moment	5.502	0.518	6.020	5.592	0.659	6.251	2.62
	$U = 3$						
Fe	3.480	0.151	3.631	3.480	0.164	3.644	
Pt	2.049	0.382	2.431	2.135	0.514	2.649	
Effective moment	5.529	0.533	6.062	5.615	0.678	6.293	2.70

4. Discussion and conclusions

We have examined the influence of different approximations (relaxed or idealized structure, local or semilocal functional, force theorem or self-consistent total-energy calculations) on density-functional calculations of the magnetic anisotropy of magnetic adatoms on Pt(111) surfaces. The surprising result of our studies is that the magnetic anisotropy energy of Fe/Pt(111) is surprisingly robust against changes in the computational setup—the results vary only between 2 and 3 meV and both easy axis orientation and the value of the MAE are in reasonable agreement with experiment [13]. For Co adatoms the variations of the MAE (between 1.2 and 12.7 meV) are much more pronounced, as a consequence of a spiky electronic density of states close to the Fermi level. But even in this case the semi-quantitative agreement with experiment is preserved, the theoretical values bracket the experimental results [4, 13]. The most important point in theoretical calculations is the description of the geometry of the adatom/substrate complex, while the remaining factors such as the choice of a functional etc are of minor importance. If relaxation is suppressed, the coupling of the magnetic adatom to the ligands with a strong SOC is strongly reduced, but this also permits the formation of a relatively large orbital moment on the adatom. If a realistic geometry is created by relaxation, the strong coupling to the ligands leads to a strong hybridization of adatom and ligand states and a larger induced moment, but the increased orbital mixing adds to the lack of orbital dependence of the exchange fields and minimizes the orbital moment of the adatom.

This important point may be illustrated by the partial local densities of states calculated for the optimized geometry of the adsorbate/substrate complex and assuming an idealized structure (see figure 3). The partial d-state densities of states (DOS) are shown for the adatom and for the atoms in the first substrate layer, for perpendicular and in-plane orientation of the magnetization. The calculations for a relaxed geometry demonstrate a strong hybridization between adatom and substrate for all states, leading to a broadening of the d states of the adatom. If an idealized geometry is assumed, the partial DOS of the d_{z^2}, d_{xy}, and $d_{x^2-y^2}$ consist of two narrow peaks located at the Fermi level and at binding energies of about −3 eV, arising from majority and minority spin states. Only the d_{xz} and d_{yz} states show a slightly stronger hybridization. The hybridization with the d band of the substrate is largely restricted to the region around the peaks in the partial Fe d-DOS. In particular, peaks just above the Fermi level are induced in the Pd d_{z^2}, d_{xz}, and d_{yz} DOS. It is also interesting to analyze the changes in the partial DOS as a function of the direction of magnetization. For perpendicular magnetization, the d_{xz} and d_{yz}, and the in-plane $d_{x^2-y^2}$ and d_{xy} states are degenerate by symmetry, for in-plane magnetization the degeneracy is lifted. As expected this splitting is more pronounced in calculations with a relaxed geometry, and—somewhat surprisingly—it is restricted to a rather narrow range of binding energies from about −4.5 to −2 eV. In this range the DOS of the d_z^2 states is more sharply peaked for out-of-plane magnetization, while for the d_{xy} and d_{yz} states whose degeneracy is also lifted, the structure in the d_{xz} DOS becomes more pronounced for in-plane magnetization while the d_{yz} DOS is more smeared out. When the partial DOSs are integrated over occupied states, the effects in the different partial DOSs largely cancel, resulting in the very small MAE of about 2 meV. The DOSs shown in figure 3 result from self-consistent calculations for both orientations of the magnetic moments—a non-self-consistent calculation with a frozen potential (as required for the use of the force theorem) gives almost identical DOS. Hence, for the elucidation of the physical mechanism determining the MAE, the partial DOSs are a too crude description of the electronic structure.

The differences in the electronic structure arising from the use of different exchange–correlation functionals on the other hand are of minor importance. The differences between the two panels of figure 3 are mostly related to the difference in the lattice constants of the substrate. The smaller lattice constant in the idealized geometry based on the smaller lattice constants calculated using the LSDA (right panel of figure 3) leads to a slightly broader Pt d band. If the Pd bands are

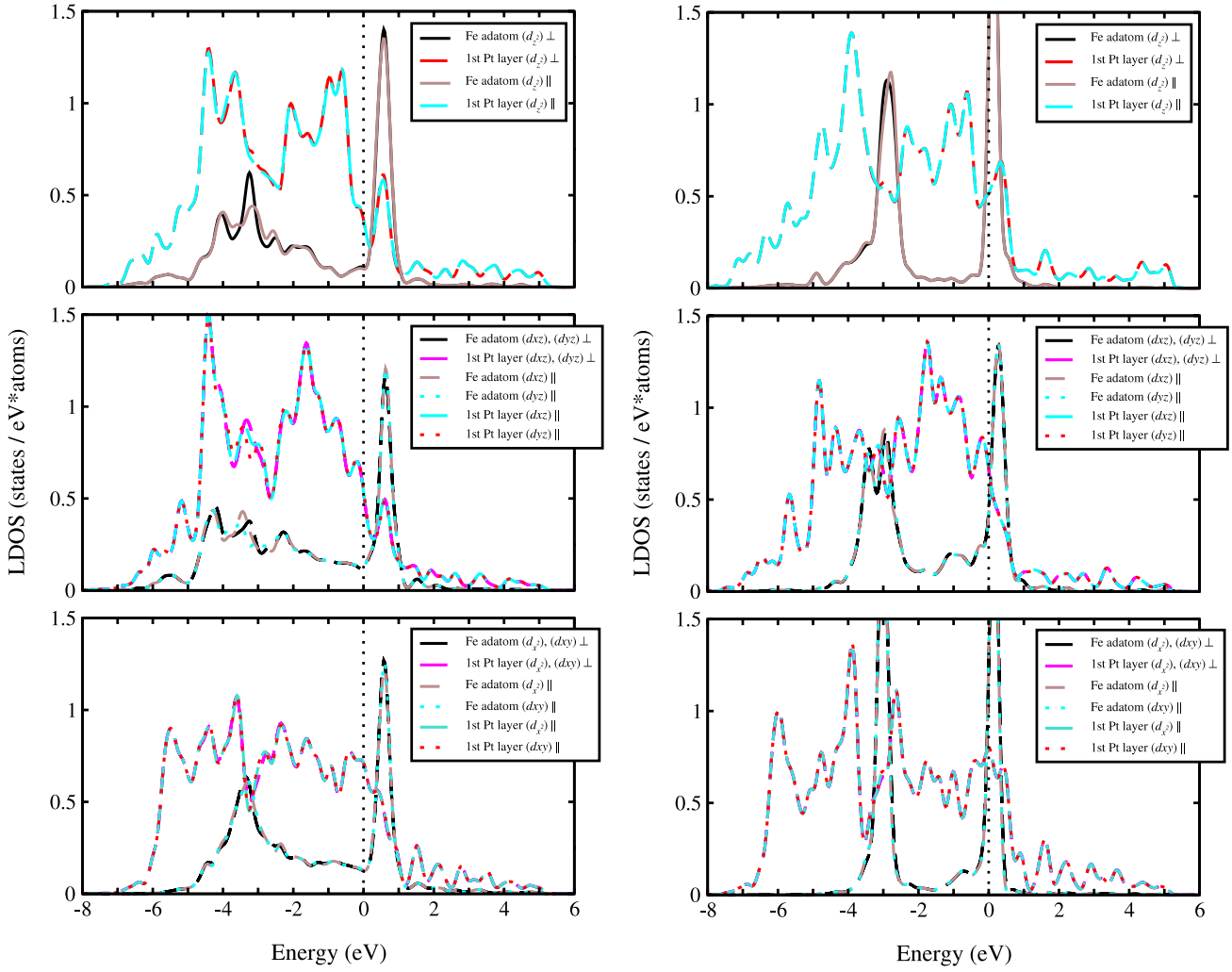

Figure 3. Partial d-electron densities of states for an Fe atom adsorbed on a Pt(111) and for the Pt atoms in the surface layer, as calculated for perpendicular and in-plane magnetization. The left panel shows the results calculated using the GGA and a fully relaxed adsorbate/substrate complex, the right one shows the results obtained using the LSDA and an idealized bulk-terminated geometry (see text).

matched at the lower band edge, the centers of gravity of the DOS for Fe majority and minority electrons are again in good agreement. An important difference—which is again mostly geometry-related—is that because of the reduced overlap of the Fe majority and minority DOSs, the Fermi level falls into a region of high Fe-DOS if an idealized geometry is used.

Altogether our analysis demonstrates that the most important approximation in DFT calculations of the magnetic anisotropy of supported nanostructures is the description of the geometry of the adsorbate/substrate complex. Calculations assuming an idealized geometry essentially attempt to cure a defect of DFT (missing orbital dependence of the exchange field) by artificially minimizing adatom/substrate hybridization. Hence while calculations based on a relaxed geometry certainly provide the more realistic scenario, both types of calculations provide a lower limit to the MAE: in one case the influence of the strong SOC on the ligands, in the other case the orbital moment of the adatom is underestimated. Future work should be based on realistic geometries and concentrate on orbital-dependent corrections to the DFT functionals, with the DFT + U being just one possible alternative. Preliminary results also demonstrate that the conclusions drawn here for isolated magnetic atoms on polarizable substrates also hold for other nanostructures (clusters, chains, ultrathin layers) composed of the same or similar elements.

Acknowledgments

This work has been supported by the Austrian Science Funds under project No. P19712-N16. We thank Anne Lehnert for communicating unpublished results and for helpful discussions.

References

[1] Sellmyer D and Skomski R 2006 *Advanced Magnetic Nanostructures* (New York: Springer)
[2] Stöhr J 1999 *J. Magn. Magn. Mater.* **200** 470
[3] Brune H and Gambardella P 2009 *Surf. Sci.* **603** 1812

[4] Gambardella P, Rusponi S, Veronese M, Dhesi S S, Grazioli C, Dallmeyer A, Cabria I, Zeller R, Dederichs P H, Kern K, Carbone C and Brune H 2003 *Science* **300** 1130
[5] Tischer M, Hjortstam O, Avranitis D, Dunn J H, May F, Baberschke K, Trygg J, Wills J M, Johansson B and Eriksson O 1995 *Phys. Rev. Lett.* **75** 1602
[6] Weller D, Stöhr J, Nakajima R, Carl A, Samat M G, Chappert C, Mégy R, Beauvillain P, Veillet P and Held G A 1995 *Phys. Rev. Lett.* **75** 3752
[7] Dürr H A, Dhesi S S, Dudzik E, Knabben D, van der Laan G, Goedekoop J B and Hillebrecht F U 1999 *Phys. Rev.* B **59** 701
[8] Gambardella P, Dallmeyer A, Maiti K, Malagoli M C, Eberhardt W, Kern K and Carbone C 2002 *Nature* **416** 301
[9] Gambardella P, Dallmeyer A, Maiti K, Malagoli M C, Rusponi S, Ohresser P, Eberhardt W, Carbone C and Kern K 2004 *Phys. Rev. Lett.* **93** 077203
[10] Koide T, Miyauchi H, Okamoto J, Shidara T, Fujimori A, Fukutani H, Amemiya K, Takeshita H, Yuasa S, Katayama T and Suzuki Y 2001 *Phys. Rev. Lett.* **87** 257201
[11] Nieuwenhuys G J 1975 *Adv. Phys.* **24** 515
[12] Meier F, Zhou L, Wiebe J and Wiesendanger R 2008 *Science* **320** 82
[13] Balashov T, Schuh T, Takacs A F, Ernst A, Ostanin S, Henk J, Mertig I, Bruno P, Miyamachi T, Suga S and Wulfhekel W 2009 *Phys. Rev. Lett.* **102** 257203
[14] Lehnert A 2009 *PhD Thesis* EPFL Lausanne
[15] Lau J T, Föhlisch A, Nietubyc R, Reif M and Wurth W 2002 *Phys. Rev. Lett.* **89** 057201
[16] Stepanyuk V S, Hergert W, Wildberger K, Zeller R and Dederichs P H 1996 *Phys. Rev.* B **53** 2121
[17] Lazarovits B, Szunyogh L and Weinberger P 2003 *Phys. Rev.* B **67** 024415
[18] Ebert H, Bornemann S, Minar J, Dederichs P H, Zeller R and Cabria I 2006 *Comput. Mater. Sci.* **35** 279
[19] Bornemann S, Minar J, Staunton J B, Honolka J, Enders A, Kern K and Ebert H 2007 *Eur. Phys. J.* D **45** 529
[20] Šipr O, Bornemann S, Minár J, Polesya S, Popescu V and Šimunek A 2007 *J. Phys.: Condens. Matter* **19** 096203
[21] Tsujikawa M, Hosokawa A and Oda T 2007 *J. Phys.: Condens. Matter* **19** 365208
[22] Etz C, Zabloudil J, Weinberger P and Vedmedenko E Y 2008 *Phys. Rev.* B **77** 184425
[23] Shick A B and Liechtenstein A I 2008 *J. Phys.: Condens. Matter* **20** 015002
[24] Hafner J and Spišák D 2007 *Phys. Rev.* B **76** 0944201
[25] Brooks M S S 1985 *Physica* B **130** 6
[26] Eriksson O, Brooks M S S and Johansson B 1990 *Phys. Rev.* B **41** 7311
[27] Anisimov V I, Zaanen J and Andersen O K 1991 *Phys. Rev.* B **44** 943
[28] Dudarev S L, Botton G A, Savrasov S Y, Humphreys C J and Sutton A P 1998 *Phys. Rev.* B **76** 195440
[29] Moroni E G, Kresse G, Hafner J and Furthmüller J 1997 *Phys. Rev.* B **56** 15629
[30] Blöchl P E 1994 *Phys. Rev.* B **50** 17953
[31] Kresse G and Joubert D 1999 *Phys. Rev.* B **59** 1758
[32] http://www.wien2k.at/
[33] Shick A B, Janis V, Drchal V and Pickett W E 2004 *Phys. Rev.* B **70** 134506
[34] Szunyogh L, Újfalussy B, Weinberger P and Kollár J 1994 *Phys. Rev.* B **449** 2721
[35] Mackintosh A R and Andersen O K 1980 *Electrons at the Fermi Surface* ed M Springfoird (London: Cambridge University Press) section 3.1
[36] Heine V 1980 *Solid State Phys.* **35** 114
[37] Kresse G and Furthmüller J 1996 *Comput. Mater. Sci.* **6** 15
Kresse G and Furthmüller J 1996 *Phys. Rev.* B **54** 11 169
[38] Perdew J P and Wang Y 1992 *Phys. Rev.* B **45** 13244
[39] Vosko S H, Wilk L and Nusair M 1980 *Can. J. Phys.* **58** 1200
[40] Kresse G and Lebacq O *VASP Manual* http://cms.mpi.univie.ac.at/vasp/
[41] Kleinman L 1980 *Phys. Rev.* B **21** 2630
[42] MacDonald A H, Pickett W E and Koelling D D 1980 *J. Phys. C: Solid State Phys.* **13** 2675
[43] Hobbs D, Kresse G and Hafner J 2000 *Phys. Rev.* B **62** 11556
[44] Marsman M and Hafner J 2002 *Phys. Rev.* B **66** 224409
[45] http://www.webelements.com
[46] Derry G N and Ji-Zhong Z 1989 *Phys. Rev.* B **39** 1940
[47] Materer N, Starke U, Barbierei A, Döll R, Heinz K, van Hove M A and Somorjai G A 1995 *Surf. Sci.* **325** 207
[48] Rohrbach A, Hafner J and Kresse G 2004 *Phys. Rev.* B **69** 075413